

MODELLING NAPL SOURCE ZONE FORMATION IN STOCHASTICALLY HETEROGENEOUS LAYERED MEDIA – A COMPARISON WITH EXPERIMENTAL RESULTS

Fritjof Fagerlund ^{1,2}
Auli Niemi ¹
Tissa Illangasekare ²

¹ Uppsala University, Dept. of Earth Sciences
Villavägen 16
75236 Uppsala, Sweden

² Centre for Experimental Study of Subsurface Environmental Processes (CESEP),
Env. Sci. and Eng., Colorado School of Mines, Golden, CO 80401-1887, USA

e-mail: Fritjof.Fagerlund@hyd.uu.se

ABSTRACT

Understanding and characterisation of subsurface occurrences of DNAPLs are important for the assessment of mass transfer from entrapped sources. Subsurface NAPL migration and the formation of immobile source zones of groundwater contamination were studied using soil flume experiments. The saturated medium is a two-layered mildly dipping system with known, stochastically generated, heterogeneity. Spatial NAPL distributions were monitored continuously using multiple energy x-ray attenuation techniques, which allows precise measurements of fluid saturations. Digital images were also taken.

Experimental results are compared to preliminary modelling results using two constitutive models: BCB by Brooks and Corey (1964) and Burdine (1953) and VGM by van Genuchten (1980) and Mualem (1976), both including a simple model of NAPL entrapment. Results indicate that the final immobile NAPL distribution is largely governed by capillary barriers during, infiltration, displacement and immobilisation of the NAPL. The description capillary pressure – fluid saturation relations is therefore a key factor in the modelling of NAPL source zone formation.

Both constitutive models reproduced the main features of the NAPL migration but overestimated immobile NAPL saturations in coarse sands enclosed by capillary barriers as well as the speed of migration. A hysteretic constitutive model is deemed likely to improve model results.

INTRODUCTION

When released at the ground surface, a DNAPL can penetrate into the saturated zone where it constitutes a long-term source of groundwater contamination. It is well documented that sub-surface heterogeneity

plays an important role in the distribution and dissolution of DNAPLs (e.g. Soga et al 2004, Saenton et al., 2002, Dekker and Abriola, 2000b, Zhu and Sykes, 2000, Powers et al. 1998, Unger et al. 1998). The sub-surface distribution of the DNAPL affects contaminant mass transfer to other fluid phases as well as the longevity and environmental impacts of a spill.

In natural systems, the migration and final distribution of DNAPLs are largely influenced by geological heterogeneity at different scales. Larger scale features such as lenses and interfaces between different sub-surface deposits may direct the general movement of mobile DNAPL and give rise to pools, perched on top of low-permeable units. On smaller scales, heterogeneity may produce preferential flow channels and control entrapment of DNAPL as blobs and ganglia. Unstable migration by fingering may also occur. Immobilisation and source zone formation has been studied experimentally in the field (Kueper et al., 1993) and in the laboratory (Ostrom et al., 1999, Illangasekare et al., 1995) as well as by numerical modelling (Dekker and Abriola 2000a, Bradford et al., 1998).

There is a significant uncertainty associated with capturing sub-surface heterogeneity through limited number of point measurements (e.g. core data). Under these conditions of uncertainty, the heterogeneity could be represented as a spatially correlated random field. A numerical model is then used to conduct Monte Carlo simulations of a DNAPL spill for different realizations of the random field. By analysing of the simulation results an understanding of the expected behaviour of the DNAPL at the site can be obtained. However, because of the complexity of NAPL migration in heterogeneous systems, it is of crucial importance that the numerical modelling codes are adequately validated for their ability to capture the dominant

processes. As comprehensive field data sets are not available, experimental data generated under controlled conditions need to be used. Gerhard and Kueper (2003a, b, c) conclude that a correct representation of constitutive relations (relative permeability – fluid saturation – capillary pressure relations) in multiphase flow simulators is a prerequisite for reliable prediction of NAPL behaviour.

However, few experimental data sets exist for numerical code validation under realistic conditions of natural heterogeneity. To characterise DNAPL source zones, heterogeneities at both small and large scales have to be considered simultaneously. Furthermore, to capture dynamic behaviour of DNAPLs in source zones, the fluid saturations need to be monitored continuously in space and time. A set of three well-controlled laboratory flume experiments were conducted to generate an accurate data set on the flow and entrapment behaviour of DNAPLs in heterogeneous systems. The tanks were packed in two distinct zones with an interface with a dip. The dip allowed for the DNAPL accumulating at capillary barriers to migrate laterally by gravity. Each experiment represented combinations of a homogenous and a heterogeneous layered formation representing a spatially correlated random field, created in the two aquifer zones.

Complete results of the experimental study are not presented here. The analysis presented in this paper is limited to the results of one of these three experiments. The goal was to test the ability of commonly used continuum-based multi-phase flow and transport models (Pruess and Battistelli, 2002, Falta et al., 1995) to capture the DNAPL behaviour in heterogeneous aquifers. The constitutive models of Brooks and Corey (1964) and Burdine (1953) (BCB-model) as well as that of van Genuchten (1980) and Mualem (1976) (VGM-model), together with a simple model for NAPL entrapment were used.

The complete data set from all three experiments will be presented in a later publication (Fagerlund et al., 2006b) followed by a more comprehensive model validation study.

THEORY AND METHODS

Experimental methods

Equivalent up-side-down setup

In the literature (e.g. Charbeneau, 2000), forces in multi-phase systems are often presented as force per unit mass. Rewriting these equations as force per unit volume for a water-NAPL system one obtains:

$$\bar{F}_n^* = (\rho_w - \rho_n)g\bar{k} - \nabla p_{cmw} - \nabla p_w \quad (1)$$

where \bar{F}_n^* , is the force per unit volume acting on the NAPL, ρ_w and ρ_n are the water and NAPL densities, g is the acceleration of gravity, \bar{k} is the upward unit vector, ∇p_{cmw} is the NAPL-water capillary pressure gradient and ∇p_w is the hydraulic pressure gradient. Consequently, neglecting the capillary pressure and hydraulic gradients, the magnitude of the vertical force is directly proportional to the density difference between NAPL and water. Now consider two water-saturated systems: one where a DNAPL moves downwards by gravity and one where a LNAPL moves upwards by buoyancy. If (i) the magnitude of the density difference $\|\rho_w - \rho_n\|$ is equal and (ii) the capillary pressure and hydraulic gradients are equivalent for the two systems, as well as (iii) other fluid properties (such as viscosity, interfacial tension, solubility etc) are the same for the DNAPL and LNAPL, then the two systems can be considered equivalent although flipped in the vertical direction. This is illustrated in Figure 1, showing a 2D-simulation (using T2VOC, Falta et al., 1995) where a DNAPL (TCE) encounters a confining layer. An LNAPL with equal $\|\rho_w - \rho_n\|$ (and other properties same as TCE) behaves exactly the same in equivalent up-side-down system.

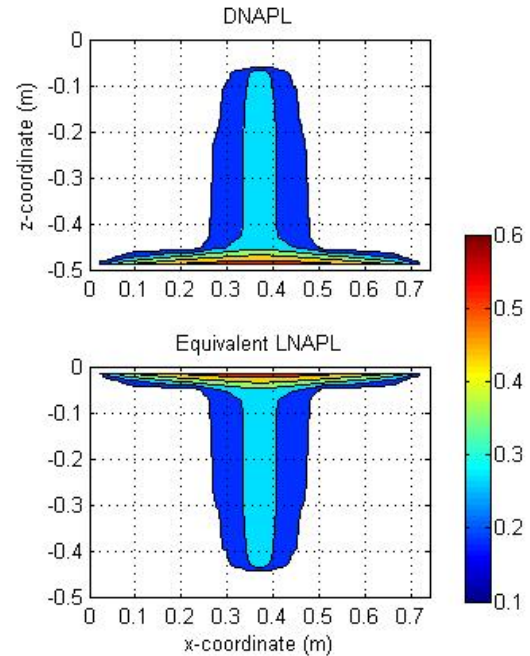


Figure 1. Simulation of downward DNAPL (TCE) migration as well as equivalent upward LNAPL migration.

Therefore, conceptually, DNAPL migration can be analysed by studying LNAPL migration in equivalent up-side-down systems. Experimentally there are several advantages of using LNAPLs. Non-hazardous DNAPLs that behave well in laboratory experiments

are not easily to find, whereas LNAPLs of low toxicity are readily available. The use of appropriate LNAPLs minimises the generation of hazardous laboratory wastes and eliminates health hazards and risk. Preparation and clean-up of equipment and test setup are safer, faster and cheaper.

Experimental flume

The experiments were performed at the Center for Experimental Study of Subsurface Environmental Processes (CESEP) at Colorado School of Mines. The experimental flume, shown in Figure 2, has inner dimensions of 71 x 53 x 4.7cm. Two constant head reservoirs at each end of the tank are used to control groundwater flow. LNAPL is injected in the lower coarser, heterogeneous layer and allowed to migrate upward towards the interface to the upper homogeneous zone with a finer soil. A slow water flow was maintained from right to left by keeping a head difference of 0.5 cm between the constant head reservoirs. A total volume of 600 mL of test-LNAPL: soltrol 220 spiked with iodoheptane (10% by weight) and coloured red with Sudan IV was injected at a constant rate of 5.302E-5 kg/s. The soltrol-mixture has density 836 kg/m³, viscosity 4.7 mNm⁻²s and interfacial tension with water $\sigma_{nw} = 0.036$ N/m.

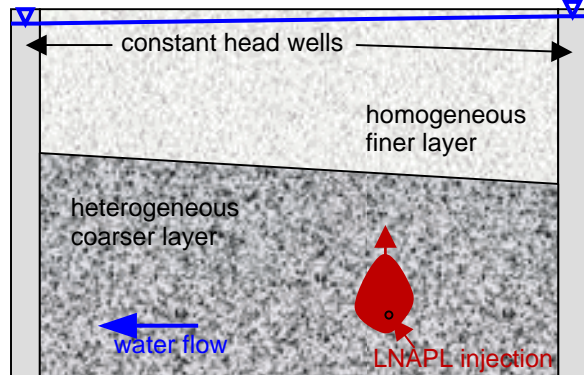


Figure 2. Experimental flume.

Heterogeneous layer

In the experiment analysed here, the lower zone of the packing, shown in Figure 3, is a heterogeneous field with mean $\ln(k) = -22.5$ and variance $(\ln k) = 1$. It was constructed using discrete blocks of five sands with known properties, given in Table 1.

Each block is 3cm in the horizontal and 1cm in the vertical direction and the field has 24 x 31 = 744 blocks. Prior to packing the flume, several heterogeneous fields were generated using correlation lengths of 6 cm and 2 cm in the horizontal and vertical directions, respectively. One of these fields, which was deemed suitable for the experiment was chosen and used in the packing. The dip of the interface between the two packing zones was set at an

angle of 3.25°, as shown schematically in Figure 2. The tank was packed wet, one horizontal layer at a time. The homogenous upper layer consisted of a mix of sands # 30 and 50. This sand mix is referred to as domain 2 in Table 1.

Table 1. Sand permeability and residual water saturations

Sand #	Domain	k (m ²)	ln(k)	S _{wr}
8	5	1.65E-09	-20.2	0.02
16	4	6.09E-10	-21.2	0.02
30	3	1.75E-10	-22.5	0.06
30&50	2	6.56E-11	-23.4	0.08
70	1	2.18E-11	-24.5	0.11

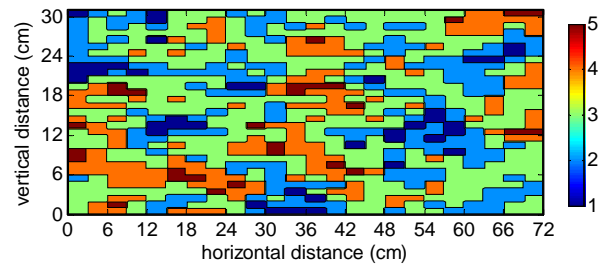


Figure 3. Lower heterogeneous zone – dark red (domain 5) is the coarsest sand, dark blue (domain 1) is the finest. In the flume, the layer is inclined 3.25°.

X-ray measurement methods

Material path lengths across the flume were measured using a multiple energy source x-ray attenuation system described in more detail by Hill III et al. (2002), Hill III (2001), Ramsey (1992). The system is automated to take point measurements at pre-programmed locations. One measurement including movement of the x-ray tube and detector using high-precision motors takes approximately 35s. Measurements of sand path lengths allow the spatial distribution of porosity to be measured before NAPL injection.

During the NAPL injection and redistribution, NAPL path lengths were measured continuously. As the movement of the NAPL slowed down, the number of measurement points was progressively increased. In the beginning some 40 points were measured (~20 minutes per scan cycle) whereas at later times measurements were taken at roughly 1800 points in space (~17 hours per scan cycle). By returning to take measurements at the same points, data on NAPL path lengths as a function of time are recorded at all measurement points. Data from one point ((x, z) =

(38.4, 18.3) (cm)) is shown in Figure 4. For any given time, the NAPL path length can be interpolated using data of the type shown in Figure 4 at all measured points, resulting in a spatial image of NAPL distribution in the flume. Using measured pore-space lengths across the tank NAPL saturations were calculated from path lengths.

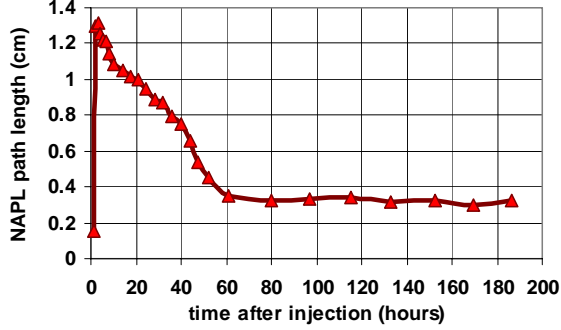


Figure 4. NAPL path length across flume at $(x, z) = (38.4, 18.3)$ (cm) as a function of time.

Numerical modelling

Numerical modelling of the experiment was performed using the compositional, non-isothermal, multi-phase flow and transport numerical simulator TMVOC (Pruess and Battistelli, 2002).

Constitutive models

Effective water saturation, \bar{S}_w , is defined as:

$$\bar{S}_w = \frac{S_w - S_{wr}}{1 - S_{wr}} \quad (2)$$

where S_w and S_{wr} are the water saturation and residual water saturation, respectively. For the Brooks-Corey (BC) model (Brooks and Corey, 1964) the relation between (NAPL-water) capillary pressure, P_{cnw} , and \bar{S}_w is:

$$\bar{S}_w = \left(\frac{P_d}{\beta_{nw} P_{cnw}} \right)^\lambda \quad (3)$$

Here P_d , the displacement pressure in an air-water system and λ , the pore-size distribution index, are BC curve-fitting parameter. β_{nw} is a scaling factor here, following Parker et al. (1987), taken as the ratio of interfacial tensions for the reference air-water system (σ_{aw}) and the NAPL-water system (σ_{nw}). Hence $\beta_{nw} = \sigma_{aw}/\sigma_{nw} = 0.072\text{Nm}^{-1} / 0.036\text{Nm}^{-1} = 2.0$. According to the van Genuchten (VG) model (van Genuchten, 1980) the corresponding relation is:

$$\bar{S}_w = \left(1 + \left(\frac{\alpha \beta_{nw} P_{cnw}}{\rho_w g} \right)^n \right)^{-m} \quad (4)$$

where α , n and m are VG curve-fitting parameters. Combining the BC-model with the relative permeability model of Burdine (1953) (BCB), including a simple model for NAPL entrapment (see Fagerlund et al., 2006 for more details), yields:

$$k_{rw} = \bar{S}_w^{3+2/\lambda} \quad (5)$$

$$k_m = \left(\frac{S_n - S_{nt}}{1 - S_{wr} - S_{nt}} \right)^2 \left[1 - \bar{S}_w^{1+2/\lambda} \right] \quad (6)$$

Here k_{rw} and k_m are the water and NAPL relative permeabilities, S_n and S_{nt} are the NAPL saturation and entrapped NAPL saturation, respectively. Note that to distinguish between different immobilisation mechanisms, we refer to immobilised non-wetting phase (NAPL) as entrapped (index t) and to immobilised wetting phase as residual (index r).

Similarly, combining the VG model with the relative permeability model of Mualem (1976) (VGM), using the same model of NAPL entrapment, yields:

$$k_{rw} = \bar{S}_w^{0.5} \left[1 - \left(1 - \bar{S}_w^{1/m} \right)^m \right]^2 \quad (7)$$

$$k_m = \left(\frac{S_n - S_{nt}}{1 - S_{wr} - S_{nt}} \right)^{0.5} \left[1 - \bar{S}_w^{1/m} \right]^{2m} \quad (8)$$

Simulation methodology

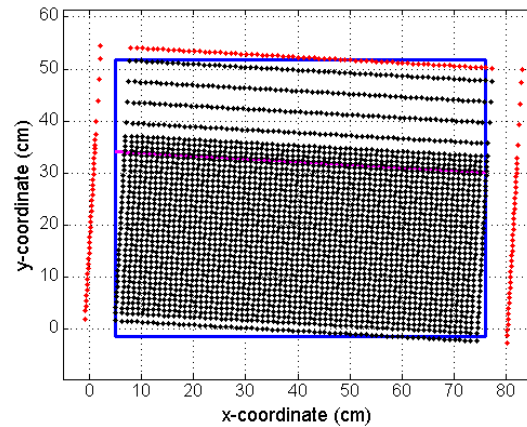


Figure 5. Centres of grid blocks used in the numerical modelling. Black: active blocks, red: const. head boundaries, blue: experiment domain, purple: sand interface.

The numerical simulations were performed using a rectangular grid aligned with the interface between the two sand zones i.e. the grid is inclined at an angle

of 3.25° with the horizontal plane. For the entire heterogeneous layer and up to 4 cm above the interface a grid spacing of 1 x 1cm was used. In the top part of the domain, where the NAPL was not observed to enter in the experiment, the spacing was 1 x 4cm. The simulation setup showing the centres of all grid blocks is given in Figure 5. In total $40 \times 70 = 2800$ active blocks (black) and 152 inactive (constituting constant head boundaries) (red) were used. Harmonic weighting of intrinsic permeabilities and up-stream weighting of mobilities (relative permeabilities) were employed.

Retention parameters

The experiment was simulated using the BCB and VGM models. For each of the five sand types, retention parameters as well as the average porosities, Φ , as measured inside the flume using the x-ray attenuation system, are given in Table 2.

Table 2. Retention parameters and average porosity.

Sand #	λ	P_d (Pa)	α^* (1/m)	n^*	S_{nt}	Φ
8	3.2	638	12	5.5	0.07	0.422
16	3	932	8.2	5.2	0.11	0.429
30	4	1668	4.8	6.6	0.15	0.443
30&50	4.6	2158	3.2	7.2	0.17	0.436
70	5.2	3924	2.2	8	0.2	0.444

* Roughly estimated values.

RESULTS AND DISCUSSION

At early times of the experiment, digital images captured the spatial NAPL saturation better than x-ray measurements. Because of the fast NAPL migration during the early period of migration, it is not feasible to take an adequate number of x-ray measurements within sufficiently short time to obtain

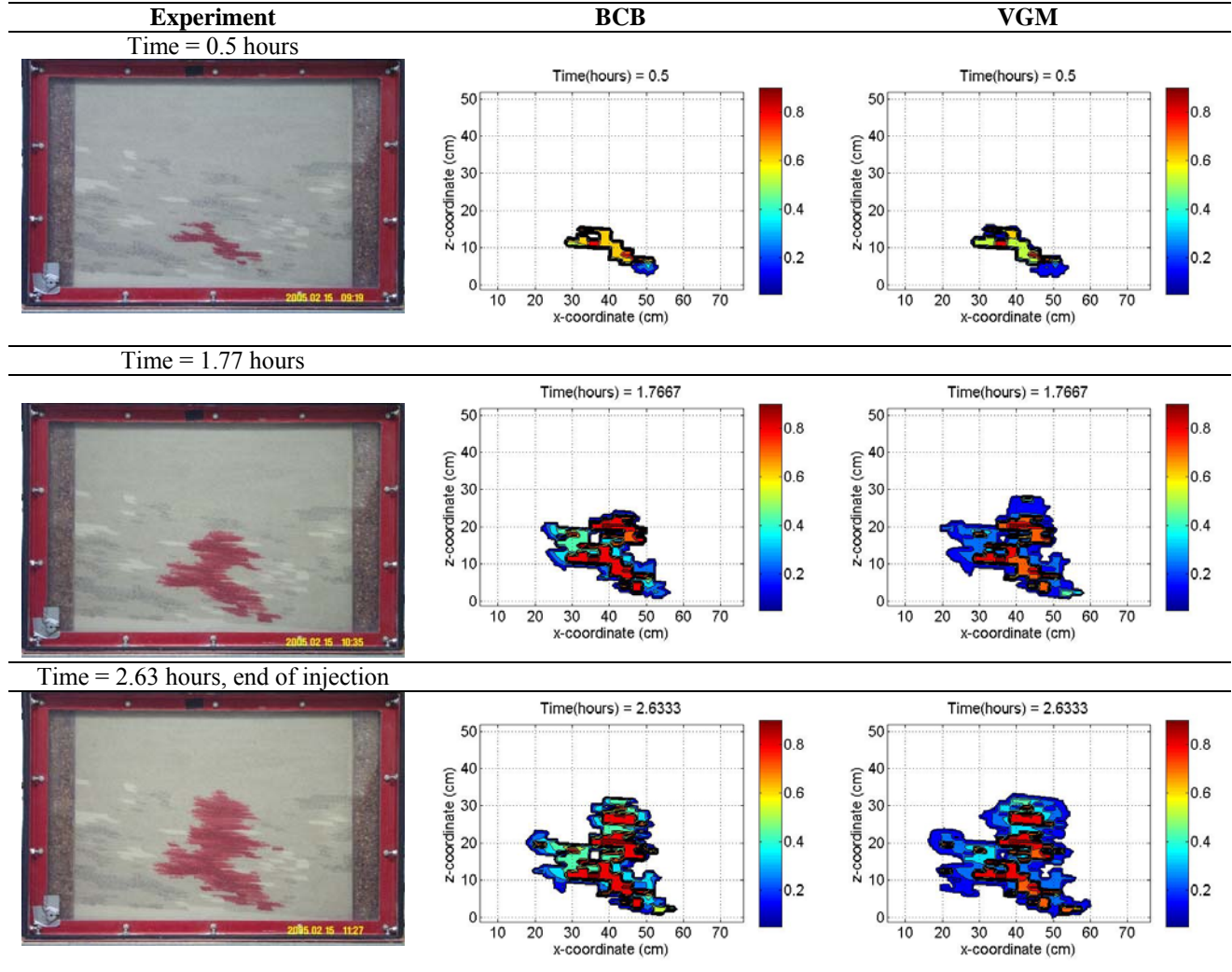


Figure 6. Spatial NAPL saturation in the experiment as digital images compared to simulated results with the BCB and VGM models.

a good spatial picture. Therefore spatial distributions of NAPL saturation during the 2.63 hour injection period were recorded using digital imaging.

Figure 6 compares experimentally observed NAPL distributions with the model simulations using BCB and VGM models, during injection. As can be seen both models capture the main features of the migration pattern at early times. Both models predict some NAPL movement to the left at an approximate elevation of $z = 20$ cm, which is not seen in the experiment. Apart from this detail, the BCB model captures the contours of the NAPL front well, whereas the VGM model predicts the NAPL plume to spread out slightly more in all directions. This is likely to be a result of the sharper entry pressure formulation of the BC- compared to the VG-model. It can also be noted that the BCB model that uses a sharp entry pressure predicts the NAPL saturations to closely follow the sand types, whereas the VGM model, that states a smoother entry of non-wetting phase into the water-saturated media, predicts somewhat more gradually changing NAPL saturations within each sand type (e.g. in the coarse sands NAPL saturations between ~ 0.65 and ~ 0.8 are predicted while the BCB model predicts ~ 0.8 everywhere where NAPL is present in coarse sand).

At later times, detailed images of the spatial NAPL saturation distribution are obtained with the x-ray attenuation system. Figure 7 shows the spatial distribution of NAPL after 12.38 hours, comparing experimental and simulated results. Here it can be seen that both predict much faster NAPL migration towards the right constant head well. In the experiment, the NAPL takes the same pathway but the migration is slower. In the experiment, the NAPL stays in the three coarsest sands i.e. # 8, 16, 30 (domains 5, 4 and 3 in Figure 3). This behaviour is predicted by the BCB model, whereas the VGM model also predicts a small amount of NAPL to enter into the mix of 30&50 sand (domain 2). The saturations in sands # 8 and 16 are better predicted by the BCB model but also reasonably well by the VGM model.

However, much smaller saturations are predicted in many locations with # 30 sand (i.e. yellow tones in the # 30 sand, seen in the x-ray plot, are not seen in the model predictions). This may be due to the fact that hysteresis is not accounted for in either of the two models. Both models use only the main drainage curves of the capillary pressure – fluid saturation functions. Hence, both models overestimate the capillary pressure between the fluid phases and the capillary drive on the water to imbibe as NAPL saturations begin to decrease. This may result in overestimation of the speed of NAPL displacement from regions from which NAPL can freely move out (i.e. usually #30 sand). Furthermore hysteresis in the

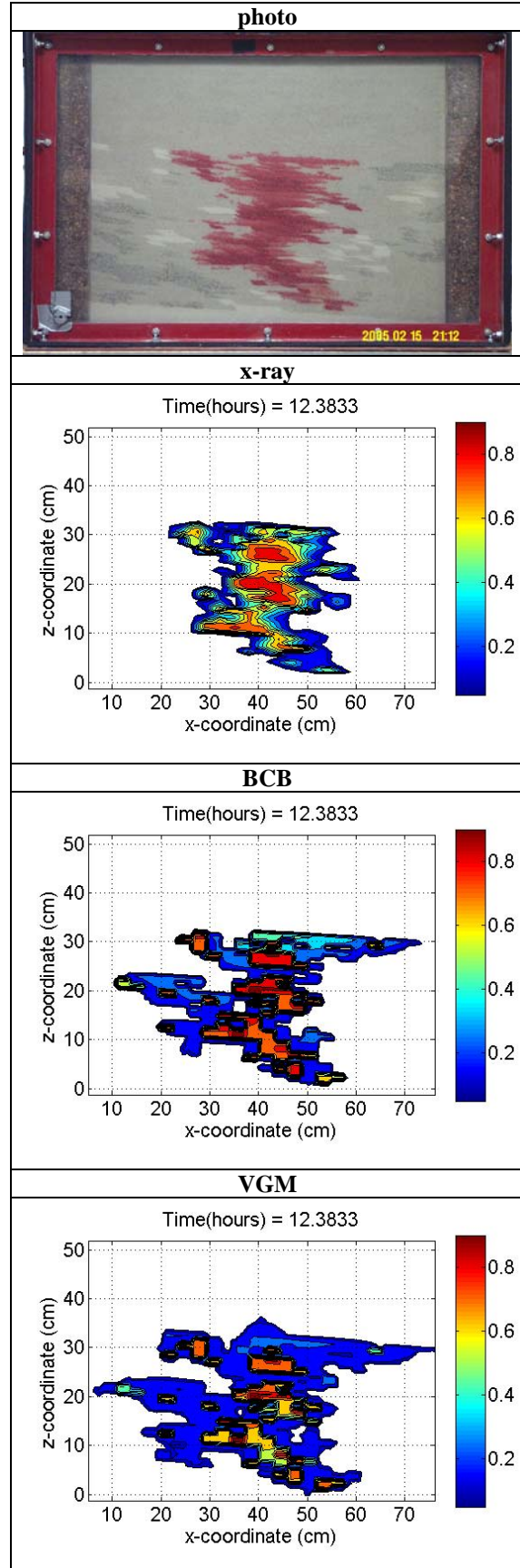


Figure 7. Spatial NAPL saturations at 12.38 hours.

relative permeability curve results in lower permeability during the imbibition cycle for most water-wet media (e.g. Gerhard and Kueper 2003c), which is not accounted for in the two models.

120 hours after the start of the experiment almost no change in spatial NAPL distribution was observed in the tank. In the spatial plot of NAPL saturation after 474 hours, shown in Figure 8 together with simulated results, all NAPL in the flume is considered immobile. Figure 8, hence, shows the observed and predicted immobilised NAPL saturations, which constitute the NAPL source zone. In the experimental flume, the NAPL remains in the three coarsest sands, where entrapment characteristics are somewhat different. In the #30 sand, the NAPL saturation is approximately 0.15 everywhere except along the interface to the upper layer where a thin pool zone of higher saturations (~0.4) is observed. This is well captured by the BCB model that also predicts saturations of 0.15 as well as a less distinct, but clearly discernible, pool zone. Also the VGM model predicts saturations of 0.15 but the NAPL is more spread out (migration into the mixed 30&50 sand occurs) and no pool in the #30 sand is predicted. In fact, very similar NAPL saturations in the #8 and #16 sands were predicted after 474 hours compared to after only 12.38 hours by both models.

In the #8 and #16 sands higher saturations were both observed and predicted due to entrapment by heterogeneities. However, after 474 hours, observed NAPL saturations have decreased substantially in the lower parts of connected units of these sands when comparing to Figure 7 (12.38 hours). This release of NAPL from the coarser sands is not predicted by any of the two models where NAPL saturations remain high everywhere, although they are somewhat lower in the lower part of the connected coarse sand units.

An overestimation of the differences in entry pressure between the coarser sands and the #30 sand during water imbibition could result in overestimation of immobilised NAPL in the coarser sand. Previous measurements by Illangasekare et al. (1995) showed that the ratio between main imbibition and main drainage displacement pressures, P_{di}/P_{dd} , was 0.71 for #16 sand and 0.63 for #30 sand, and ratio of the difference in displacement pressures ($(P_{di,30} - P_{di,16}) / (P_{dd,30} - P_{dd,16})$) was 0.57. Recent measurements of the main drainage curve (shown in Table 2), show that the retention properties of the sands have undergone some change since they were previously measured. Nonetheless, it seems reasonable to assume that for imbibition, the difference in entry pressures between sands #30 and 16 should be in the order of 60% of the difference during drainage. This results in a less pronounced capillary barrier at sand interfaces during imbibition compared to during drainage. The assumption is also supported in general

by P_{di}/P_{dd} ratios for a number of sands given by Gerhard and Kueper (2003b).

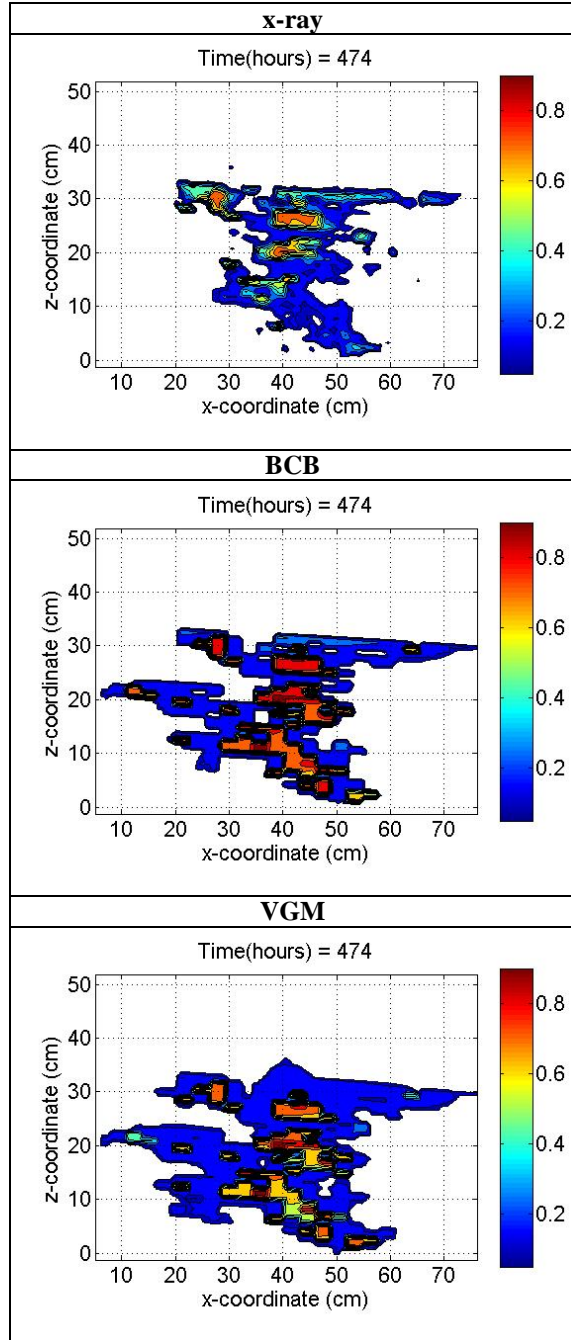


Figure 8. Spatial NAPL saturations at 474 hours.

The VGM model predicts slightly lower NAPL saturations in the #8 and #16 sands compared to the BCB model which agrees somewhat better with the observed immobile saturations after 474 hours. This is likely due to the fact that the VG capillary pressure – saturation curve is smoother at low non-wetting phase saturations.

CONCLUDING REMARKS

NAPL migration in layered, stochastically heterogeneous media has been studied using a high precision flume experiment and compared to numerical simulations. Preliminary modelling results show that the two tested constitutive models, VGM and BCB with the inclusion of a simple entrapment model, were able to capture the main features of the NAPL migration. The speed of migration as well as immobilised NAPL saturations in the coarser sands were, however, overestimated by both models. A model that includes hysteresis in the capillary pressure and relative permeability functions is believed to improve the agreement between observed and simulated results.

Immobile NAPL constitutes a source zone for groundwater contamination. In heterogeneous media, the final, immobile, spatial distribution of NAPL saturations is largely governed by capillary pressure heterogeneities at material interfaces. The results indicate that capillary forces during drainage large controls into where the NAPL can penetrate and the shape of the NAPL plume (reproduced well by the drainage-based constitutive models). During imbibition of water capillary barriers control how much NAPL can be displaced and how much is immobilised. Consequently, capillary pressure – fluid saturation relations for both the imbibition and drainage cycles are of key importance for predictions of NAPL source zone architecture.

For homogeneous regions of the medium, from which NAPL can be displaced without crossing a capillary barrier, a simple entrapment model, using a constant NAPL entrapment saturation, agrees well with experimental data.

ACKNOWLEDGMENTS

The authors thank the Swedish Rescue Services Agency (Räddningsverket), the Swedish Road Department (Vägverket) and the U.S. National Science Foundation (award number DMS-0222286) for providing funding for this research. Furthermore, F. Fagerlund thanks Dr. T. Sakaki and Dr. M. Komatsu for measurements of sand permeabilities and capillary pressure – fluid saturation curves, K. Glover, D. Rodrigues and J. Gago for training and assistance with the x-ray attenuation measurement system and Dr. M. Mathew for assistance with flume packing and modelling.

REFERENCES

Bradford, S. A., L. M. Abriola and K. M. Rathfelder, Flow and entrapment of dense nonaqueous phase liquids in physically and chemically

- heterogeneous aquifer formations, *Adv. Water Resour.*, 22(2), 117-132, 1998.
- Brooks, R. H. and A. T. Corey, Hydraulic properties of porous media, Hydrology paper 3, Colorado State University, Fort Collins, Colorado, 1964.
- Burdine, N. T., Relative permeability calculations from pore size distribution data. *Trans. Am. Inst. of Mining and Met. Engineers*, 198, 71-78, 1953
- Charbeneau, R. J., *Groundwater hydraulics and pollutant transport*, Prentice Hall, New Jersey, USA, 2000.
- Dekker, T. J. and L. M. Abriola, The influence of field-scale heterogeneity on the infiltration and entrapment of dense nonaqueous phase liquids in saturated formations, *J. Contam. Hyd.*, 42, 187-218, 2000a.
- Dekker, T. J. and L. M. Abriola, The influence of field-scale heterogeneity on the surfactant-enhanced remediation of entrapped nonaqueous phase liquids, *J. Contam. Hyd.*, 42, 219-251, 2000b.
- Fagerlund, F., A. Niemi and M. Odén, Comparison of relative permeability – fluid saturation – capillary pressure relations in the modelling of non-aqueous phase liquid infiltration in variably saturated, layered media, Article in Press, *Adv. Water Resour.*, 2006a.
- Fagerlund, F., A. Niemi and T. H. Illangasekare, NAPL migration and source zone formation in heterogeneous layered media: 1 Experimental investigation, Manuscript under preparation, 2006b.
- Falta, R. W., K. Pruess, S. Finsterle and A. Battistelli, *T2VOC User's Guide*, Report LBL-36400, UC-400, Lawrence Berkeley National Laboratory, Berkeley, Calif., 1995.
- Gerhard, J. I. and B. H. Kueper, Capillary pressure characteristics necessary for simulating DNAPL infiltration, redistribution and immobilization in saturated porous media, *Water Resour. Res.*, 39(8), 1212, 2003a.
- Gerhard, J. I. and B. H. Kueper, Relative permeability characteristics necessary for simulating DNAPL infiltration, redistribution and immobilization in saturated porous media, *Water Resour. Res.*, 39(8), 1213, 2003b.
- Gerhard, J. I. and B. H. Kueper, Influence of constitutive model parameters on the predicted migration of DNAPL in heterogeneous porous media, *Water Resour. Res.*, 39(10), 1279, 2003c.
- Hill, E. H. III, L. L. Kupper and C. T. Miller, Evaluation of path-length estimators for characterizing multiphase systems using polyenergetic x-ray absorptiometry, *Soil Sci.*, 167(11), 703-719, 2002.
- Hill, E. H. III, *User's Manual for V2.0 of the CMR X-ray Attenuation Analysis Programs*, Unpublished Report, Center for Multiph. Res., Dept., Env. Sci. Eng., Univ. N. Carolina, Chapel Hill, NC, 2001.

- Illangasekare, T. H., J. L. Ramsey Jr., K. H. Jensen and M. B. Butts, Experimental study of movement and distribution of dense organic contaminants in heterogeneous aquifers, *J. Contam. Hydrol.*, 20, 1-25 1995.
- Kueper, B. H., D. Redman, R. C. Starr, S. Reitsma and M. Mah, A field experiment to study the behavior of tetrachloroethylene below the water table: Spatial distribution of residual and pooled DNAPL, *Ground Water*, 31(5), 756-766, 1993.
- Mualem, Y., A new model for predicting the hydraulic conductivity of unsaturated porous media, *Water Resour. Res.*, 12, 513-522, 1976.
- Oostrom, M., C. Hofstee, R. C. Walker and J. H. Dane, Movement and remediation of trichloroethylene in a saturated heterogeneous medium 1. Spill behavior and initial dissolution, *J. Contam. Hyd.*, 37, 159-178, 1999.
- Parker, J. C., R. J. Lenhard and T. Kuppusamy, A parametric model for constitutive properties governing multiphase flow in porous media, *Water Resour. Res.*, 23, 618-624, 1987.
- Powers, S. E., I. M. Nambi and G. W. Curry Jr., Non-aqueous phase liquid dissolution in heterogeneous systems: Mechanisms and a local equilibrium modeling approach, *Water Resour. Res.*, 34(12), 3293-3302, 1998.
- Pruess, K., and A. Battistelli, *TMVOC, A Numerical Simulator for Three-Phase Non-Isothermal Flows of Multi-Component Hydrocarbon Mixtures in Saturated-Unsaturated Heterogeneous Media*, Report LBNL-49375, Lawrence Berkeley National Laboratory, Berkeley, Calif., 2002.
- Ramsey, J. L. Jr., Experimental investigation of dense organic contaminant transport through heterogeneous porous media, M.Sc. thesis, Dept. of Civil Eng., Colorado School of Mines, Colorado, USA, 1992.
- Saenton, S., T. H. Illangasekare, K. Soga and T. A. Saba, Effects of source zone heterogeneity on surfactant-enhanced NAPL dissolution and resulting remediation end-points, *J. Contam. Hyd.*, 59, 27-44, 2002.
- Soga, K., J. W. E. Page and T. H. Illangasekare, A review of NAPL source zone remediation efficiency and the mass flux approach, *J. Haz. Materials*, 110, 13-27, 2004.
- Unger, A. J. A., P. A. Forsyth and E. A. Sudicky, Influence of alternative dissolution models and subsurface heterogeneity on DNAPL disappearance times, *J. Contam. Hyd.*, 30, 217-242, 1998.
- van Genuchten, M. T., A closed-form equation for predicting the hydraulic conductivity of unsaturated soils, *Soil Sci. Soc. Am. J.*, 44, 892-898, 1980.
- Zhu, J. and J. F. Sykes, The influence of NAPL dissolution characteristics on field-scale contaminant transport in subsurface, *J. Contam. Hyd.*, 41, 133-154, 2000.